Lab on a Chip

PAPER

View Article Online
View Journal

Cite this: DOI: 10.1039/d4lc00911h

A new biofunctionalized and micropatterned PDMS is able to promote stretching induced human myotube maturation†

Théo Regagnon,[a] Fabrice Raynaud,[b] Gilles Subra,[c] Gilles Carnac,[b] Gerald Hugon,[b] Aurélien Flatres,[a] Vincent Humblot,[d] Laurine Raymond,[c] Julie Martin,[c] Elodie Carretero,[c] Margaux Clavié,[c] Nathalie Saint,[b] Sylvie Calas,[a] Cécile Echalier,[c] Pascal Etienne[a] and Stefan Matecki *[be]

Inter-individual variability in muscle responses to mechanical stress during exercise is poorly understood. Therefore, new cell culture scaffolds are needed to gain deeper insights into the cellular mechanisms underlying the influence of mechanical stress on human myogenic progenitor cells behavior. To this end, we propose the first *in vitro* model involving uniaxial mechanical stress applied to aligned human primary muscle-derived cells, employing a biocompatible organic–inorganic photostructurable hybrid material (OIPHM) covalently attached to a stretchable PDMS support. Using a laser printing technique with an additive photolithographic process, we optimally micropatterned the PDMS support to create longitudinal microgrooves, achieving well-aligned muscle fibers without significantly affecting their diameter. This support was biofunctionalized with peptide sequences from the ECM, which interact with cellular adhesion receptors and prevent myotube detachment induced by stretching. X-ray photoelectron spectroscopy (XPS) of biofunctionalized PDMS with RGD-derived peptide deposition revealed a significant increase in nitrogen compared to silicon, associated with the presence of a 380 nm thick layer measured by atomic force microscopy (AFM). Upon cell culture, we observed that functionalization with an RGD peptide had a beneficial impact on cell fusion rate and myotube area compared to bare PDMS. At the initiation of the stretching protocol, we observed a three-fold rapid and transient increase in RNA expression for the mechanosensitive ion channel protein piezo and a decrease in the ratio of nuclei expressing myogenin relative to the total nuclei count (43 ± 16% *vs.* 6 ± 6%, $p < 0.01$). Compared to day 0 of differentiation, stretching the myotubes induced MHC and Titin colocalization (0.66 ± 0.13 *vs.* 0.93 ± 0.05, $p < 0.01$), favoring sarcomere organization and maturation. In this study, we propose and validate an optimized protocol for culturing human primary muscle-derived cells, allowing standardized uniaxial mechanical stress with a biocompatible OIPHM covalently linked to PDMS biofunctionalized with an ECM-derived peptide, to better characterize the behavior of myogenic progenitor cells under mechanical stress in future studies.

Received 30th October 2024,
Accepted 22nd January 2025

DOI: 10.1039/d4lc00911h

rsc.li/loc

Introduction

Many pathological conditions (*e.g.*, myopathies, cancer, diabetes) and non-pathological conditions (*e.g.*, sedentary lifestyle, bed rest, immobilization, space flight) lead to a loss of muscle mass and consequent reduction in functional capacity and life expectancy.[1,2] Regular physical activity remains the most effective preventive measure,[3] with mechanical stimuli induced by exercise being essential for maintaining skeletal muscle balance.[4] Indeed, stretching protocols on muscle fiber cultures, mimicking *in vitro* the physiological conditions experienced during exercise, promote maturation and contractile function.[5–7] However, there is significant variability in how individuals' muscles respond to exercise training and the cellular mechanisms underlying this variability are poorly understood. To specifically evaluate the myogenic progenitor response to mechanical stress induced by exercise it is necessary to develop new scaffolds for cell

[a] *Laboratoire Charles Coulomb, CNRS UMR 5221, Université de Montpellier, CC 074, Place E. Bataillon, F-34095 Montpellier, France*
[b] *PhyMedExp, CNRS, INSERM, University of Montpellier, F34295 Montpellier, France. E-mail: stephan.matecki@umontpellier.fr*
[c] *IBMM, CNRS, ENSCM, University Montpellier, Montpellier, France*
[d] *CNRS, FEMTO-ST, Université Franche-Comté, F-25000 Besançon, France*
[e] *Service de Physiologie CHU Arnaud de Villeneuve Montpellier, France*
† Electronic supplementary information (ESI) available. See DOI: https://doi.org/10.1039/d4lc00911h

culture that allow fine-tuned, homogeneous stretching of aligned human myotubes, derived from skeletal muscle biopsies.

Indeed, when myotubes are cultivated directly on bare surfaces, as is usually the case on Petri dishes, they tend to arrange randomly, leading to varying mechanical stress levels across different fibers. This causes random cell fusions that can result in aberrant proliferation and differentiation.

Considering that myotube alignment in culture leads to more advanced fiber differentiation,[8,9] several techniques, including hydrogel anchoring,[10,11] 3D-bioprinting,[12,13] micro-contact printing[14,15] or electrospinning,[16,17] have been developed to achieve aligned myotubes.

Thanks to these advancements, organs-on-chips have become promising alternatives to traditional two-dimensional (2D) cell or animal model for biological research or drug screening.[18] Furthermore, for treating functional tissue loss, the musculoskeletal system or liver are considered potential candidates for exogenous vascularized muscle or liver-on-chip transplantation.[19–21]

In regard to muscle applications, while these techniques have demonstrated efficacy in obtaining aligned muscle fibers, none is sufficiently expandable to withstand the range of tension necessary for mechanistic research purposes to model *in vitro* mechanical stretching induced by exercise.[22] Indeed, during exercise, the variations in stretch imposed on a muscle fiber can range from simple stimulation beneficial for muscle growth to the induction of lesions with higher tension ranges, as observed, for example, in athletes with exercise-induced damage.[23]

Polydimethylsiloxane (PDMS), also known as silicone, exhibits interesting mechanical properties for stretching myotubes in cell culture and commercial devices specifically designed for stretching muscle fibers in culture use it. However, PDMS must be micropatterned to force cultured myogenic progenitors to differentiate along a longitudinal axis. The surface geometry of PDMS can be modified using micro molding,[24] laser ablation,[25] or micro-wrinkling.[26]

However, micro-wrinkling is poorly reproducible, and the laser ablation process is complex to master. Even though the use of micro-molding[27–29] is largely preferred, it requires repeated master mold fabrication for each new geometry. Therefore, we are always reliant on manufacturing technologies that are expensive due to the necessity of creating a master mold, and unsuitable for rapid prototyping.

This last point is very important, and our objective is to propose a new tool that easily allows the modification of mechanical stress input and the guidance of muscle fibers, facilitating the comparison, even simultaneously, of responses to a range of mechanical constraints in human primary myoblast-derived myotubes. Additionally, replication problems necessarily arise over time due to master wear.

A promising alternative considered in our study is laser printing using an additive photolithographic process, requiring the deposit of a photostructurable polymer such as SU-8 resin on PDMS. SU-8 resin is commonly used in many biomedical applications, including scaffolds for cell culture and cell encapsulation.[30,31] However, SU-8 has poor adhesion on PDMS, even after oxidation with O_2 or air plasma, resulting in a high risk of detachment when stretching.[32]

Considering that plasma processes generate hydrophilic Si–OH groups on the PDMS surface, we firstly hypothesized that preparing a biocompatible organic–inorganic photostructurable hybrid material (OIPHM) on plasma-treated PDMS *via* the sol–gel process would significantly increase adhesion to PDMS through covalent siloxane bonds.[33]

Hybrid materials have been extensively studied for several years, including for medical applications.[34] There are primarily two processes for photocrosslinking the organic part of OIPHM: free radical or cationic photoinitiators. The first process typically uses methacrylates or acrylate groups. The main issue with free radicals, especially in coating processes, is the inhibition caused by the presence of oxygen. Consequently, the polymerization process is incomplete, and the final properties are not maximized.[35]

Moreover, despite the presence of the inorganic part, low adherence on silicon and silica has been reported.[36] For several years, we have developed a synthesis based on a new generation of organic–inorganic materials, where the organic part is photopolymerized using a cationic method, which is known to be insensitive to oxygen.[33,37] Epoxy groups are good candidates because of their low shrinkage during polymerization and their good adherence to various substrates.[38] We chose 2-(3,4-epoxycyclohexylethyltrimethoxysilane) (EETMOS) due to its very high reactivity and high conversion rate.[39]

The primary benefit of this technique lies in its capacity to generate diverse patterns with varying widths and heights of the microgrooves, facilitating the identification of optimal dimensions to obtain perfectly aligned and well differentiated muscles fibers. Indeed, the specific attributes of micropatterning that enable the cultivation of well-aligned muscle fibers without notably influencing their diameter remain unidentified.

Additionally, even micropatterned, PDMS must also be biofunctionalized to enhance cell adherence. Oxidizing the surface using O_2 or air plasma is unsatisfactory due to its reversible nature after a brief period,[40,41] leading to potential cell or myotube detachment during stretching protocols. Hydrogel coating is commonly used to biofunctionalize PDMS,[42] but despite covalent binding with O_2 plasma pre-treatment, adhesion is variable, with poor mechanical stress transmission to muscle fibers in the hydrogel.

In this study, we propose covalent binding of a peptide from the ECM, interacting with cellular adhesion receptors, such as sequences like RGD or YIGSR[43,44] or IKVAV,[45] as a promising alternative. Considering the successful use of these peptides in various cells,[46,47] we hypothesize that a micropatterned PDMS biofunctionalized with RGD sequences will enhance myoblast adhesion, ensuring optimal adherence of myotubes during stretch protocols. This scaffold could

optimally evaluate the stretch-induced behaviors of myogenic progenitors.

Thus, the first objective of the present study is to propose, for the first time to our knowledge, a micro-patterning technique and biofunctionalization of PDMS surfaces based on UV additive photolithography of hybrid precursor EETMOS (2-(3,4-epoxycyclohexylethyltrimethoxysilane)) followed by the deposition of a hybrid RGD-derived peptide.

Considering that the height and width of the guide grooves can be easily modulated with this technique, our second objective is to determine the optimal dimensions to generate well-differentiated and aligned myotubes derived from human primary muscle cells. Finally, the last objective of this study is to propose the first *in vitro* model involving uniaxial mechanical stress applied to human primary muscle-derived cells, employing biocompatible organic–inorganic photostructurable hybrid material (OIPHM). The specificity of our model would be, for future studies focused on the behavior of myogenic progenitors induced by mechanical stress, to be able to apply a wide range of tensions enabling the modeling of mechanical stretching induced by exercise, ranging from simple beneficial stimulation for muscle growth to the induction of pathological lesion processes.

Materials & methods

Extendable scaffold for cell culture

EETMol sol synthesis. [2-(3,4-Epoxycyclohexylethyltrimethoxysilane)] (EETMOS) and 1-methoxy-2-propanol (Dowanol®) were purchased from Sigma-Aldrich. Hydrochloric acid (0.1 N) was purchased from Honeywell International Inc. Omnirad CPTX and Omnicat 250 were purchased from IGM resins. The sol synthesis protocol is described in a patent[48] and a previous study.[33] Briefly, EETMOS was mixed in 99% pure ethanol (0.8 m/m of EETMOS). A 1/10 EETMOS/water molar ratio was used to initiate the hydrolysis reaction. A 0.1 N aqueous hydrochloric acid solution was added dropwise into the EETMOS/ethanol solution under acidic conditions to favor hydrolysis over condensation. The solution was closed and stirred for 4 hours at 60 °C. This solution was then concentrated at 60 °C using a rotavapor, gradually reducing the pressure to reach a 75% wt concentration. This step serves two objectives: (1) to eliminate residual water that could interfere with epoxy polymerization and (2) to increase viscosity for achieving the desired deposit thickness on the silicon membranes.

In parallel, Omnirad CPTX and Omnicat 250 were solubilized in Dowanol® to reach a 1.5% w/w and 5% w/w ratio with EETMOS, respectively. Omnirad CPTX, a thioxanthone derivative, has a peak absorption at 375 nm and produces a radical compound upon excitation, which activates Omnicat 250, a cationic photoinitiator. This combination is necessary because Omnicat 250 absorbs light most effectively at 250 nm, not aligning with the UV laser used in our process. The solution was stirred in an ultrasound bath for 30 minutes at 50 °C, then stirred for 4 hours. Post sol concentration, 30% wt of this solution was mixed with Dowanol® (35% w/w with EETMOS) to obtain a yellow viscous mixture. This sol (EETMol) can be stored at −15 °C for several weeks.

Plasma activation and film deposition

Silicone bare membranes were obtained from Flexel International (Burlington, NC, USA). They were treated with a Diener electronic plasma system using 100% oxygen flow at 0.6 mbar, a 13.56 MHz excitation frequency, and a power of 80 W for 3 minutes. The silicone membrane was homogeneously covered with EETMol using a spin coater from Suss Microtech, rotating at 3250 rpm for 20 seconds (acceleration 1000 rpm s^{-1}, deceleration 500 rpm s^{-1}). This setting was optimized to obtain an 8–10 μm thick film, hypothesizing that such microstructure thickness could guide myotube development without restraining their transverse diameter. Indeed, Xu *et al.*[49] previously showed that even a 400 nm deep nanostructure is sufficient to align myotubes. The film was then pre-baked for 5 minutes at 50 °C.

Micropatterning and microscopic characterization

To rapidly optimize micropatterning geometry, a maskless photolithographic process using laser writing technology was chosen. The Dilase 650 (KLOÉ France) equipped with a 375 nm laser with 100 mW max intensity (spot diameter: 2 μm) was used. A network of parallel lines with the desired width and spacing was sketched using KLOÉ SA software. After the drawing process, the substrates underwent a "post-exposure bake" for 15 minutes at 80 °C to promote epoxy polymerization and crosslinking of the insolated resin parts. The membranes were then washed in an isopropanol bath, dissolving the non-polymerized areas and revealing the parallel microgrooves. Finally, the microstructured membranes were heated at 130 °C for 3 hours to improve adhesion and complete polymerizations of the organic and inorganic parts of EETMol. These microstructured membranes can be stored at room temperature indefinitely. The samples were observed with a VHX 7000 digital microscope (Keyence) to verify that the height, spacing, and width of the microgrooves met expectations. Mechanical properties were obtained using an ultra-nanoindenter system (UNHT from Anton Paar) on 10 measurements. The mean Young's Modulus value is 5.27 ± 0.03 GPa and the mean Hardness value is 324 ± 2 MPa with 95% confidence (Student's *t*-distribution).

Biofunctionalization with silylated peptides

The syntheses of bis-silylated RGD and RAD peptides were carried out following a methodology previously described by our group,[50] detailed in ESI† (Fig. C and Materials and methods). Briefly, peptides were synthesized *via* standard solid-phase peptide synthesis (SPPS) using the Fmoc/*t*Bu strategy on a 2Cl chloro trityl PS resin. After cleavage with a

trifluoroacetic acid (TFA) cocktail, the primary amine group of the N-terminus and the primary amine of the C-terminal lysine side chain of each peptide were reacted with isocyanatopropyl triethoxysilane (ICPTES) in dimethylformamide (DMF) in the presence of diisopropylethylamine (DIEA). Notably, using one equivalent of ICPTES per amino function allowed selective reaction with the primary amine, leaving the serine alcohol side chain unreacted. Hybrid peptides were isolated by precipitation in diethyl ether and stored under vacuum. The peptides were weighed and solubilized in a 1% aqueous solution of TFA/ethanol (15/85) to obtain concentrations of 1, 10, and 20 mg mL^{-1} (0.97, 9.7, and 19.3 mmol L^{-1}, respectively). The silicone membranes (micropatterned or not) were activated by plasma treatment (100% O_2; 0.6 mbar; 13.56 Hz; 80 W; 1 min) to generate silanol groups on the surface. These groups reacted with the hybrid peptides, forming siloxane (Si–O–Si) covalent bonds during the dip-coating process (up and down speed of 5 cm min^{-1}). The peptide-functionalized membranes were then left at 50 °C for 24 hours to accelerate the condensation process between the hybrid peptides and the silicone. Non-covalently attached peptides were removed by washing in a water/ethanol solution (30/70). Due to the covalent nature of the grafting, these membranes were stable in air or in solution at neutral pH and could be stored for weeks.[51] To verify the efficiency of the biofunctionalization process of our PDMS membranes with silylated peptides, X-ray photoelectron spectroscopy (XPS) and atomic force microscopy (AFM) analyses were performed.

-XPS analysis. XPS analyses were performed using a Thermo Fisher Alpha 110 photoelectron spectrometer, equipped with a non-monochromated AlKα radiation source ($h\nu$ = 1486.6 eV) and a 300 W electron beam power. The emission of photoelectrons from the sample was analyzed at a takeoff angle of 90° under ultra-high vacuum conditions ($\leq 10^{-9}$ mbar). Spectra were acquired with a 100 eV pass energy for the survey scan and a 20 eV pass energy for the C 1s, O 1s, S 2p, and N 1s regions. Binding energies were calibrated against the C 1s (C–C) binding energy at 284.8 eV, and element peak intensities were corrected by Scofield factors.[52] The peak areas were determined after subtraction of a Shirley background. Spectra were fitted using Casa XPS v.2.3.15 software (Casa Software Ltd, U.K.) with a Gaussian/Lorentzian ratio of 70/30.

AFM analysis. The surface morphology of the biofunctionalized PDMS membranes was characterized using an atomic force microscope Step 700 (Anton Paar GmbH, Austria) operating in air under ambient conditions. Measurements were carried out in tapping mode on a scan area fixed at 20 μm × 20 μm.

Primary cultures of human myoblasts. Quadriceps muscle biopsies were performed at the Centre Hospitalier Universitaire Montpellier on healthy adults (AFM-BTR "Banque de tissus pour la recherche"). Briefly, myoblasts from biopsies were purified following the protocol optimized in our laboratory[53] and frozen until use. After an ethanol wash of the substrates, 10^5 cells were seeded on micropatterned membranes of varying sizes in DMEM/F12 (Dulbecco's modified Eagle medium/nutrient mixture F-12) with 10% fetal calf serum (FCS), 0.1% Ultroser G, and 0.1% human basic FGF (growth medium) at 37 °C in 95% humidified air with 5% CO_2. After 3 days of proliferation, confluent myoblasts were cultured for differentiation in DMEM high glucose with 5% FCS for 4 days. A similar protocol was used on bare membranes to serve as a reference.

Immunofluorescence. Myotubes obtained from primary cultures were fixed in 2% paraformaldehyde (Electron Microscopy Sciences, Ayguesvives, France) in PBS (phosphate buffer saline) and permeabilized with PBS + 0.25% Triton X-100 at room temperature. Cells were then incubated with mouse monoclonal anti-troponin T (1/200; Sigma-Aldrich) or mouse monoclonal anti-α-actinin (1 : 200; Sigma-Aldrich). Secondary antibody was goat anti-mouse Alexa Fluor® 647 (1 : 100; Thermo Fisher Scientific). Nuclei were revealed by DAPI staining. Images were taken with a Zeiss epifluorescence and LSM800 confocal microscope and then analyzed with ImageJ software. DAPI and troponin-T-positive cells were analyzed using Fiji software to obtain the number of nuclei and the total myotube area per image, normalized to the total image area to compare all conditions. The fusion index was calculated as the ratio of the number of nuclei in troponin-T positive cells with ≥3 nuclei to the total number of nuclei. To measure the diameter of the myotubes, straight lines were drawn perpendicular to each myotube on troponin-T-positive cells. When a consistent difference in diameter was observed on one myotube, multiple lines were drawn to assess the mean diameter. For each myotube, the length of each line and its deviation from the longitudinal axis of the microstructures were also measured.

Stretching protocol. Primary human myoblasts were seeded on biofunctionalized microstructured PDMS membranes until confluence. The culture medium was changed to induce differentiation and, 2 days later, the membranes with the differentiated myotubes were meticulously transferred into the uniaxial MCT6 stretching apparatus (CellScale, Waterloo, Canada). The stretching program consisted of a 1 hour stimulation followed by a 2 hour rest, repeated once per day for two days. The stretching amplitude was set at 0.2 mm, approximately 10% of the medium myotube length measured by immunofluorescence, and the frequency was set at 1 Hz.

RNA expression. The impact of our stretch on myogenic progenitor cells differentiation was evaluated with RNA expression measurement for piezo, a protein related to mechanotransduction pathways, myogenic regulatory factors, and sarcomeric organization. For longitudinal analysis, muscle fibers subjected to the stretching protocol were removed at 6 different time points and frozen in "RNA later" solution (Life Technologies). Results were compared with unstretched fibers. Tissues were then dissociated in RLT buffer using a fast prep homogenizer (MP Biomedicals).

Reverse transcription reactions were performed on 500 ng total RNA using a reverse transcription Takara Kit (Takara Bio Europe), and real-time quantitative PCR was performed with the Lightcycler 480 II real-time PCR instrument (Roche). Primer pairs were generated using the NCBI primer design application and were designed to span an exon–exon junction. Forward and reverse primer sequences (presented in ESI† Materials and methods) were used at specific annealing temperatures. Data on gene expression were normalized according to RPLP0 housekeeping gene expression.

Sarcomere protein organization assessment and colocalization. We evaluated the impact of our stretching protocol on sarcomere organization by immunofluorescence. Muscle fibers were stained with titin and MHC1 antibodies to assess the level of colocalization of these two main sarcomeric proteins with the Zeiss LSM 800. All cell conditions at different time points of the stretching protocol were observed with the same microscope settings (laser intensity, pinhole). We used the Coloc 2 module from Fiji, a plugin for colocalization analysis, which performs pixel intensity correlation methods of Pearson, Manders, Costes,

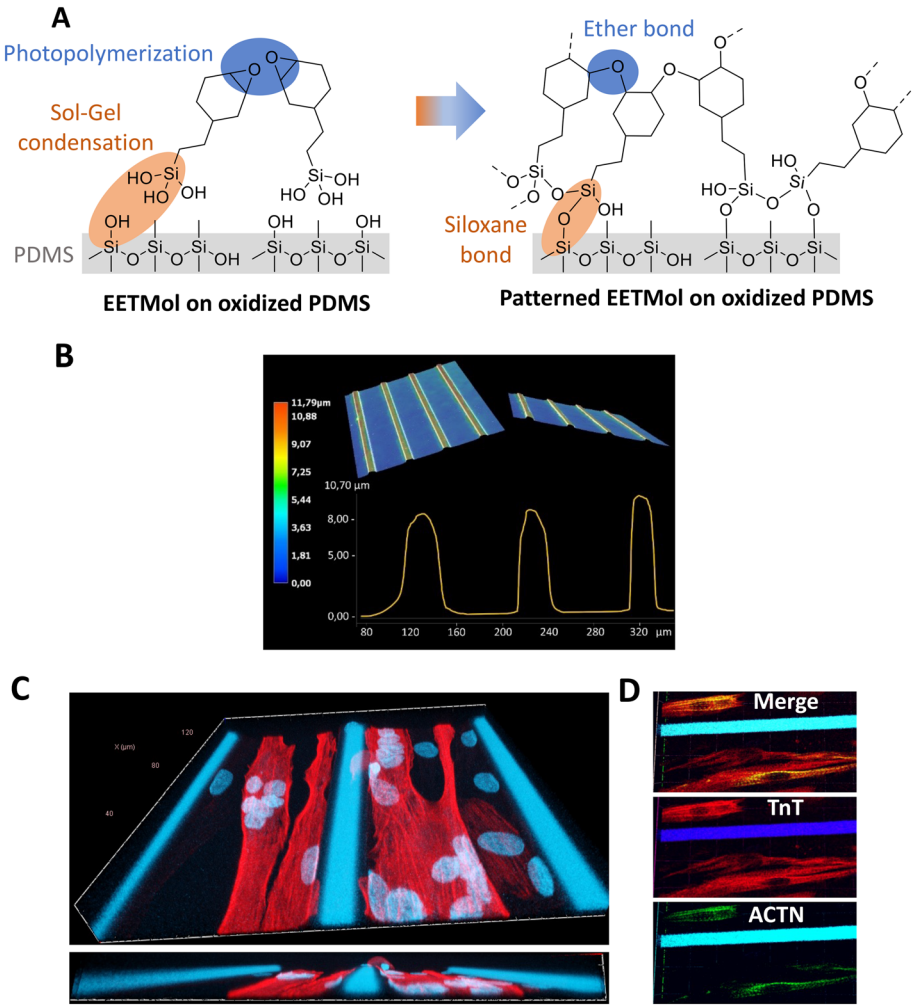

Fig. 1 Characterization of the line network of EETMOS microstructured PDMS membranes and confocal imaging with myotubes in culture. Panel A) Schematic representation of EETmol functions to prepare microstructures immediately after deposition on PDMS (left side) and after all curing processes (right side). The condensation reaction between the silanol groups of EETmol and the oxidized PDMS, resulting in siloxane bonds, is circled in red. Additional siloxane bonds arise from the condensation reaction between the silanol groups of two adjacent EETmol molecules. Blue ellipses indicate the polymerization process of epoxy groups under irradiation, which contributes to the microstructure through ether bonds. Notice that we have deliberately zoomed in on the interface. It is obvious that there are still several unreacted silanol groups in the layer. Panel B) EETMOS polymerization is activated by UV photolithography, and the micropatterned membranes are observed under a microscope. A 3D representation of the line network with topographic analysis by optical profilometry is shown. The topographic analysis confirms the precision of the microstructures, although the curve shape shows small height variations between 8 and 9.5 µm. This variation is due to the film deposition, which was not always completely homogeneous across the entire membrane area. Panel C) Confocal imaging of the system with the micropatterns (lines in blue), myotubes stained in red with troponin T (TnT), and nuclei stained with DAPI (in blue). The lower panel is a transversal slice showing the relationship between the cells and the micropattern. Panel D) Pre-sarcomeric structure revealed by anti-actinin antibody (ACTN) in green.

Li, and more, for scatterplots, analysis, automatic thresholding, and statistical significance testing. The point spread function (PSF) was set at 3, and the randomization cost at 20. We used Spearman's rank correlation as a colocalization marker. For fluorescence intensity, we used the red, green, and blue (RGB) profiler from Fiji.

Statistics. Statistical significance was determined using the *t*-Student test where $p < 0.05$ (*) was considered significant. Two-way ANOVA was used to compare kinetic RNA expression between stretched and unstretched groups. $p < 0.05$ (*) was considered significant, and each time point corresponded to an experiment repeated in duplicate. Error bars represent the standard deviation of the mean. A Kolmogorov–Smirnov test was performed for the analysis of myotube deviation from the mean orientation axis.

Results & discussion

Biocompatibility of EETMol micropatterns

EETMol, which exhibits high adhesion to PDMS, appears to be a promising alternative to SU-8 for providing a structurable layer with UV additive photolithography. However, it has never been tested for cell culture. In the first step, as shown in ESI† Fig. A, we demonstrated that EETMol, compared to SU-8, is not cytotoxic for human primary cell cultures and has similar biocompatibility.

The EETMol solution contains silanol groups (Si–OH) (Fig. 1A, left panel). When deposited, these groups allow both adhesion to the oxidized PDMS membrane, thanks to the formation of siloxane covalent bonds (Si–O–Si) through the sol–gel process (water condensation reaction), and an increase in the mechanical properties of the microstructures due to the mineral nature of the siloxane bond (Fig. 1A, right panel). Additionally, the EETMol solution contains epoxy rings (Fig. 1B, left panel). After deposition, these rings are locally polymerized under UV irradiation to form ether bonds and build microstructures (Fig. 1A, right panel).

EETMol microstructures on the PDMS membranes were imaged with a digital microscope. A 3D representation of the line network was obtained after topographical analysis by optical profilometry, as shown in Fig. 1B. The analysis confirmed the precision of the microstructures, although the curve shape showed small height variations between 8 to 9.5 μm. This variation was due to the film deposition, which was not always entirely homogeneous across the whole area of the membrane.

Interestingly, we observed with confocal microscopy, as shown in Fig. 1C and D, that the myotubes expanded horizontally, following the longitudinal axis of the microstructure. They attached to the wall rather than remaining centrally within the grooves. This "edge effect", previously described,[54] could be attributed to the presence of adhesion sites that mimic the microenvironment observed *in vivo*. Indeed, extracellular matrices that interact with myogenic progenitors produce patterns of mechanical constraint, forcing them to proliferate and differentiate in regions of concentrated growth along the longitudinal axis.[55] Before any stretching protocol, we also observed the presence of α-actinin staining, which indicates the initiation of maturation marked by the presence of striated myotubes (Fig. 1C).

Influence of the grooves spacing and height on cell fusion rate, myotube diameter, and alignment

It is widely acknowledged that surface topography significantly influences myotube differentiation and alignment.[8,9] Therefore, our aim was to determine the optimal dimensions for micropatterns to achieve a 2D culture of myotubes that are aligned and tightly organized along a single axis, resembling the *in vivo* configuration. To achieve this goal, we modified the microstructure pattern with photolithography to create four samples with varying spacing between the micropattern edges: 25 μm, 50 μm, 75 μm, and 100 μm, while maintaining a height of 8 μm. These dimensions were chosen based on the average diameter of myotubes obtained *in vitro* from muscle biopsy.[56] A fifth sample, consisting of a bare PDMS membrane, served as a negative control. All samples were coated with a 3 μm Matrigel® layer to facilitate myoblast adhesion to the scaffold. Myoblasts were seeded in each culture condition at a consistent density (refer to the methodology section).

To validate the quality of muscle fiber alignment, we quantified the myotube mean orientation deviation as a function of micropattern spacing (Fig. 2). This outcome is illustrated in Fig. 2A, showing the presence of non-aligned myotubes up to 30° with 100 μm edge spacing compared to 50 μm spacing. As quantified in Fig. 2B, we observed an increase in non-aligned myotubes with increasing edge spacing. Interestingly, our results showed that the cell fusion rate and myotube area were proportional to the pattern spacing (Fig. 2C and D).

After 3 days of cell differentiation, we compared the effect of the spacing on the cell fusion index (Fig. 3A), myotube area (Fig. 3B), and mean diameter (Fig. 3C). Compared to the bare PDMS membrane, we observed a statistically significant increase in the cell fusion index for all micropatterned supports, reaching the highest rate with a 25 μm spacing between the micropattern edges (52 ± 4% *vs.* 79 ± 2%, $P < 0.05$) (Fig. 3A). As shown in Fig. 3B, we obtained similar results regarding the myotube area, with almost three times higher values compared to control for 25 μm spacing (531 741 ± 69 580 *vs.* 1 372 138 ± 114 760 μm^2, $P < 0.05$). Moreover, we did not observe a statistical effect of micropattern height on myotube area, cell fusion index, or mean diameter (Fig. 3D and ESI† Fig. B).

Our results indicate that micropatterning enhances both the cell fusion rate and myotube area, with a beneficial reduction in the distance between the edges of the micropatterns. This underscores the influence of

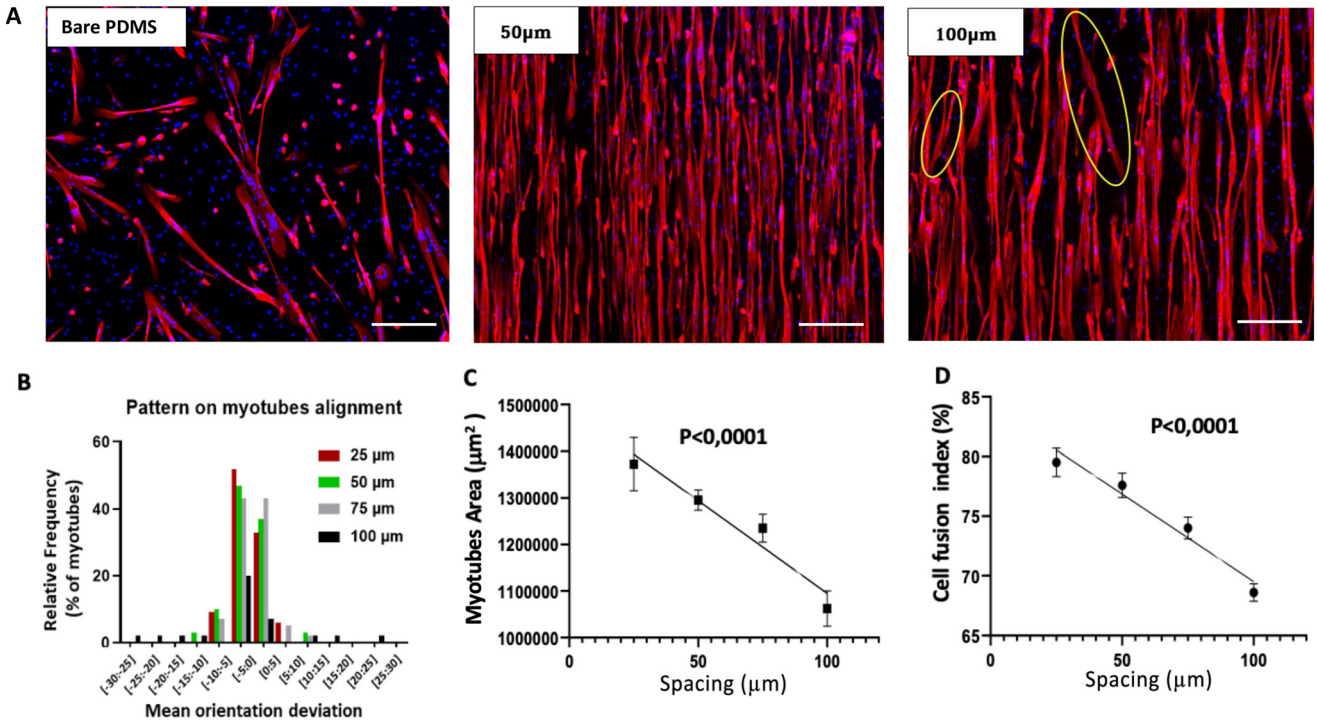

Fig. 2 Micropatterns lead to cell alignment. Panel A) Immunofluorescence of a bare PDMS membrane (left panel), micropatterns with a 50 µm spacing (middle panel), and micropatterns with a 100 µm spacing (right panel). The yellow circles represent the major deviations from the mean orientation axis. Panel B) Effect of the spacing on myotube alignment. Panel C and D) Inverse correlation between the spacing and cell fusion rate (right panel), and myotube area produced (left panel). Scale bar: 200 µm.

topographic constraints on myotube differentiation, as previously observed.[9,55] Mechanical inputs induced by reducing the distance between the edges are converted into signaling events that elicit biological responses through mechanically activated (MA) ion channels, which include a large family of ion channels.[57] However, compared to the bare PDMS, except for the smallest spacing between the micropattern edges (25 µm), we observed that micropatterned supports have no effect on the mean diameter of myotubes. Indeed, for a spacing of 25 µm, corresponding to the highest level of topographic constraints, the mean myotube diameter was statistically lower compared to the bare PDMS (19.3 ± 0.7 µm *vs.* 27.3 ± 2.8 µm, $P < 0.05$). Our results highlight the importance of an optimal balance between the mechanical inputs necessary to stimulate muscle fiber maturation and the necessary space between the microgrooves for fiber growth. Based on our results, a 25 µm spacing between the edges appears optimal for fiber differentiation. However, this small gap stimulates muscle fiber growth on the longitudinal axis at the expense of transverse diameter. Therefore, we propose a 75 µm spacing as an optimal balance between increasing the transverse myotube diameter while maintaining well-aligned fibers along a single longitudinal axis. These results show for the first time, to our knowledge, that topographic constraints can induce mechanical inputs, guiding the alignment and maturation of human primary myoblast-derived myotubes.

Biofunctionalization of the optimal micropatterned support for stretching protocol

To avoid any myoblast-derived myotube detachment during the stretching protocol, biofunctionalization of the microstructured PDMS is necessary. To this end, we decided to covalently attach the RGD peptide sequence, present in the ECM,[43] to our PDMS membrane to increase cell adhesion. A control peptide was synthesized where glycine from the RGD motif was replaced with alanine, preventing the recognition of the sequence by integrins. Functionalization of the microstructured PDMS with the RAD peptide served as a negative control in the biofunctionalization test.

Triethoxysilane groups were introduced on the RGD or RAD sequence to allow the formation of siloxane bonds with the microstructured PDMS *via* the sol–gel process. We previously described the functionalization of biomaterials with a mono-silylated peptide sequence.[50] Here, we synthesized bis-silylated peptides to form a covalent 3D network on the PDMS surface (ESI† Fig. C).

To verify the grafting of the peptides to the PDMS surface, XPS analyses were conducted on five distinct samples: bare PDMS, three samples functionalized with the RGD peptide at varying concentrations (1 mg mL^{-1}, 10 mg mL^{-1}, and 20 mg mL^{-1}), and one sample with RAD peptide at 10 mg mL^{-1}. As shown in ESI† Fig. D, in all five samples, the trio of carbon (C 1s), silicon (Si 2p), and oxygen (O 1s) characteristic of PDMS is present. Nitrogen (N 1s) appears only in the

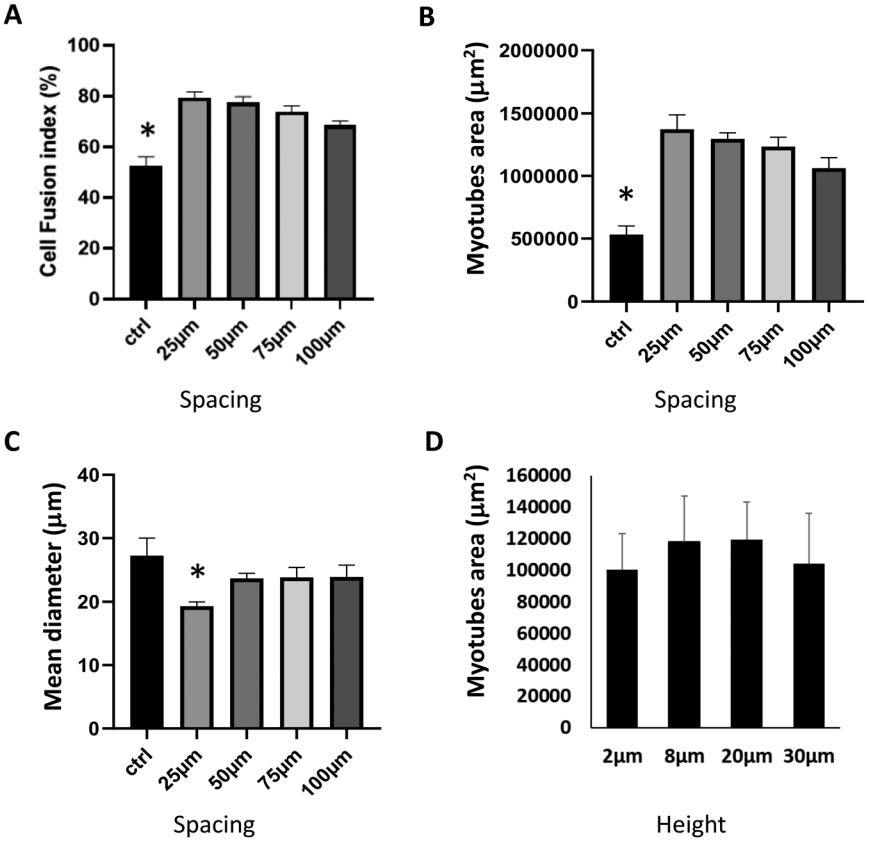

Fig. 3 Effect of micropattern spacing on: panel A) cell fusion rate, panel B) myotube area, panel C) mean diameter of the myotubes. Panel D) Effect of micropattern height on myotube area. $p < 0.05$ (*).

biofunctionalized samples. Interestingly, when the RGD peptide concentration exceeds 1 mg mL^{-1}, the presence of nitrogen increases while that of silicon decreases, indicating the formation of a peptide layer.

We measured the thickness of the RGD peptide coating on PDMS with AFM analysis. As shown in Fig. 4A, we observed a layer of 150 nm with a 10 mg mL^{-1} RGD peptide solution and a layer of 380 nm with 20 mg mL^{-1}, in favor of a covalent 3D network on the PDMS surface with bis-silylated peptides.

Finally, we evaluated the impact of PDMS biofunctionalization with RGD peptide at different concentrations on myogenic progenitor cells' behavior following 3 days of proliferation and 3 days of differentiation, using the same methodology as previously described. As shown in Fig. 4B, compared to bare PDMS, the RGD peptide has a beneficial impact on cell fusion rate and myotube area, with an optimal effect at the highest peptide dose (20 mg mL^{-1}). This result suggests a higher number of accessible adhesion sites on PDMS for the myotubes, resulting in more advanced differentiation.

XPS and AFM analyses confirmed the functionalization of the PDMS with the bis-silylated RAD control peptide (ESI† Fig. D and E). However, as expected, the RAD peptide did not impact the differentiation of the myotubes (ESI† Fig. F), demonstrating that the beneficial effect observed with the RGD peptide is specific to the peptide sequence.

To better evaluate the interest of adhesive peptides such as RGD, we compared the effect of four different culture conditions of myogenic progenitor cells (bare PDMS, microstructured bare PDMS, microstructured PDMS with RGD, and microstructured PDMS with RGD and Matrigel) following 3 days of proliferation and 3 days of differentiation on cell fusion index and myotube area. The results presented in ESI† Fig. G show that microstructuring by itself and coatings have a beneficial effect on myotube differentiation compared to bare PDMS. However, there was no significant difference between RGD and RGD + Matrigel on microstructured PDMS. These results indicate that RGD coating is as effective as Matrigel in promoting myotube maturation.

More over, to test the stability of the coating over the time, we evaluated the effect of a 18 month old PDMS coated with bisylated peptide on myotube differentiation in comparison to bare PDMS (Ctr). As showed in the Fig. H in ESI,† we found that the coating still favors cell attachment and myotube differentiation attested by a significant increase of cell fusion index, myotube area and nuclear number in coated PDMS condition. The RGD on the PDMS is therefore stable over time.

Our results showed that matrigel could be successfully replaced by covalent binding of biopolymers or peptides from the ECM, which have the main advantage to interact with

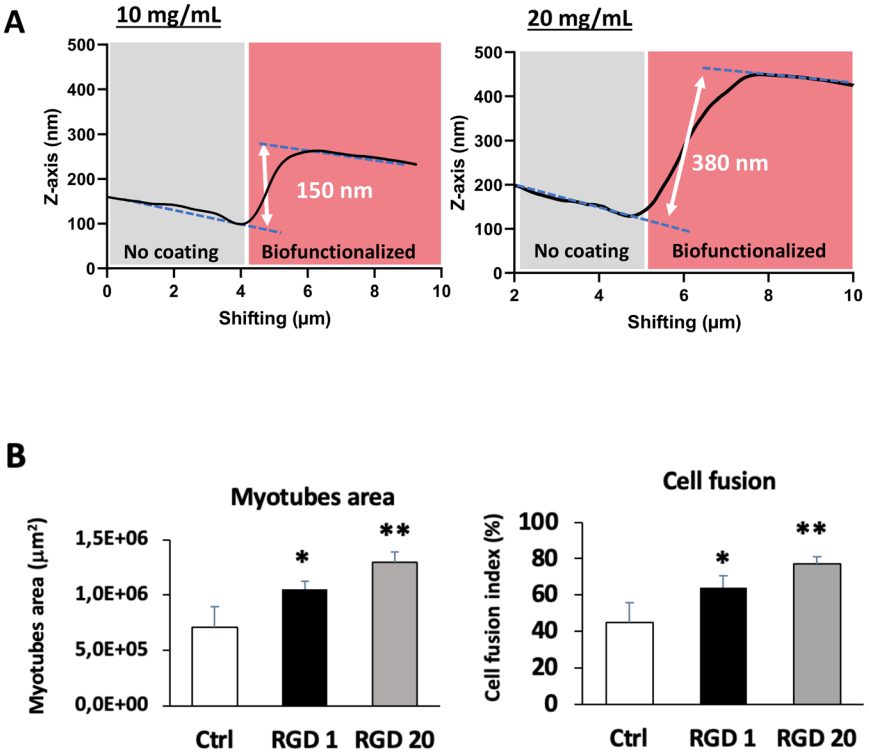

Fig. 4 Biofunctionalization by peptide-grafting on PDMS. Panel A) Effect of peptide concentration on myotube area and cell fusion rate, panel B) AFM characterization of the surface of a PDMS membrane biofunctionalized with a 10 mg mL^{-1} (left panel) or 20 mg mL^{-1} (right panel) peptide solution.

cellular adhesion receptors and prevent myotube detachment induced by stretching. Moreover, most *in vitro* cell cultures use coatings with collagen and Matrigel matrices derived from animals, particularly mice and rats. In addition to ethical concerns, the use of animal matrices does not allow for standardization of experiments (technical constraints)

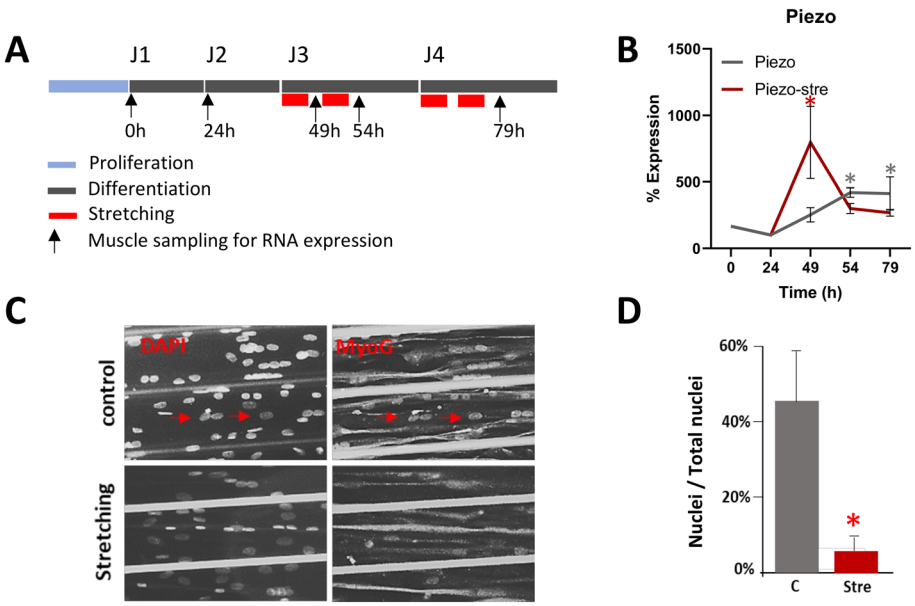

Fig. 5 Stretching induces myotube differentiation. Panel A) Stretching protocol, panel B) comparison of piezo RNA expression kinetics in stretched *versus* unstretched conditions, panel C) effect at the H54 time point of the stretching protocol on the number of nuclei expressing MyoG relative to the total nuclei count, panel D) effect of the stretching protocol on MyoG immunostaining and DAPI compared to control conditions (n = 2 in each group, $p < 0.05$).

and is more susceptible to damage by stretching protocols. These synthetic alternatives could enhance cell adhesion to the support, resistance to stretching mimicking exercise, and repeatability of the experiments.

Stretch-induced behaviors of human myogenic progenitors

Mechanical stress promotes the proliferation, differentiation, and maturation of myogenic progenitors, allowing for the maintenance of skeletal muscle balance.[4,5] Thus, we aimed to verify whether our *in vivo* model of unidirectional mechanical stress would result in aligned and well-differentiated human myotubes. The first step was to establish a well-defined mechanical stimulation protocol regarding the stretching amplitude of the muscle fiber as a percentage of its initial length, duration, and timing of initiation. Each of these parameters has been independently investigated in previous studies and has demonstrated an influence on myotube differentiation.[58,59] However, *in vitro* mechanical stress protocols to enhance myotube maturation are not standardized, and none have been evaluated on human aligned myotubes so far. The protocol consisted of two stretching cycles initiated 48 h (J3) and 72 h (J4) after the differentiation period. Each cycle, lasting 4 hours, consisted of two periods of one-hour stretching separated by 2 hours without any stretch (Fig. 5A). This protocol resulted from several tests and adjustments (data not shown) to optimize the proliferation and differentiation of our human myogenic progenitors. The stretching amplitude was set at 0.2 mm, corresponding to 10–15% of the average myotube length, a range commonly used to induce myotube differentiation in numerous previous studies.[5,6,58–67]

To confirm that myotubes experienced mechanical stress and responded accordingly, we monitored the impact of stretching by measuring RNA expression of piezo, a mechanosensitive protein on the cell membrane involved in transmitting mechanical stretch to induce cellular responses related to myogenic progenitor differentiation.[57,68] Five specific time points were selected for analysis: the first at confluence (J1) when differentiation was induced, the second after 24 hours (J2), the third at J3, just after 1 hour of stretching (49 h time point), the fourth also at J3, just after the first stretching cycle (54 h time point), and the last at J4, after the second stretching cycle (79 h time point). Results were compared with unstretched controls. In line with previous observations,[68,69] we observed a three-fold rapid and transient increase in myotube piezo RNA expression immediately after 1 hour of stretching (49 h time point), followed by a rapid decrease below the unstretched condition level at 54 h and 79 h time points (Fig. 5B).

To verify whether our stretching model could activate human myotube differentiation, we evaluated, at 54 h, just after the first stretching cycle, compared to unstretched myotubes, the number of nuclei expressing MyoG, a crucial transcriptional myogenic regulatory factor for skeletal muscle determination and terminal differentiation,[70] relative to the total nuclei count. We observed that stretched myotubes had a significantly lower ratio of nuclei expressing this transcription factor compared to total nuclei (6 ± 6% *vs.* 43 ± 16%, $p < 0.01$) (Fig. 5C and D), illustrating the termination of the differentiation program induced by mechanical stress, a process that occurred earlier than in the unstretched control group.

To attest to the beneficial impact of our longitudinal stretching protocol on human myotube maturation at the

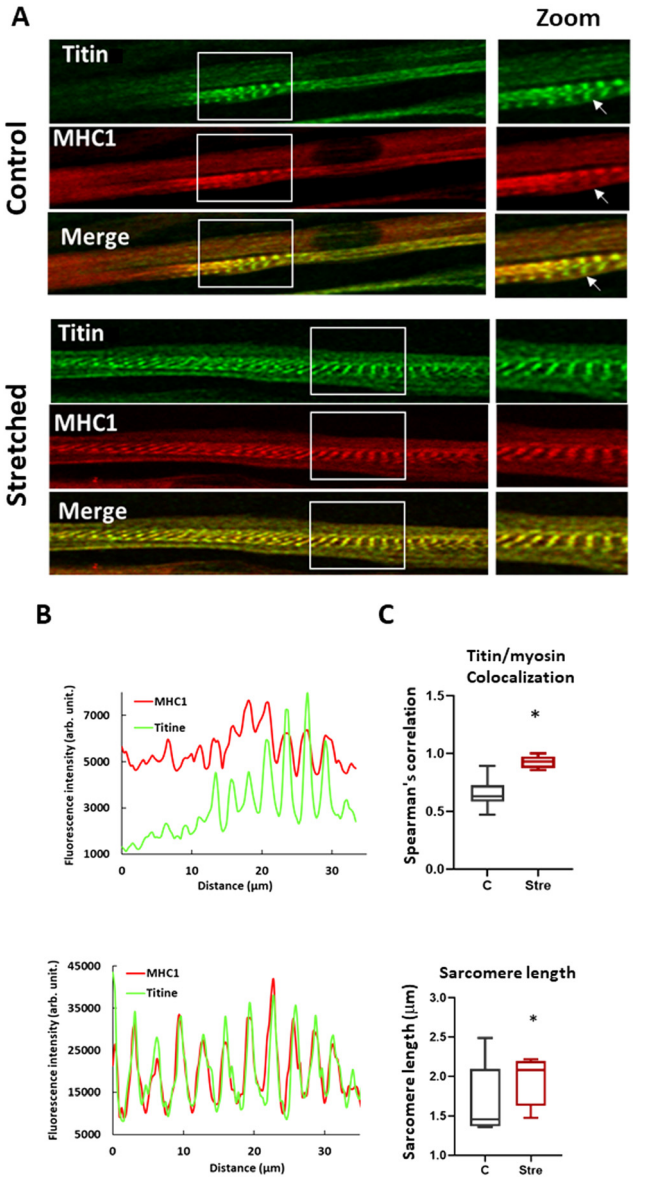

Fig. 6 Stretching induces sarcomeric maturation. Panel A) Confocal immunofluorescence staining of titin and MHC 1 in stretched and unstretched human myotubes. The arrow in the unstretched myotube shows the absence of MHC 1 in a sarcomeric structure, indicating a lower level of sarcomeric maturation, panel B) the graph shows the fluorescence profile of titin and MHC 1 when a line is drawn in the muscle fiber, panel C) percentage of colocalization between titin and MHC 1 staining (upper panel) and the effect of stretching on sarcomere length compared to control (lower panel). $p < 0.05$ (*).

protein level, we compared stretched myotubes stained with Titin and MHC1 antibodies after one cycle to unstretched conditions by immunofluorescence. As illustrated in Fig. 6A, the stretching condition showed improved sarcomere organization with well-defined striation, corroborating results from previous studies on murine myoblast cell lines.[71,72] Sarcomere organization was characterized by quantifying MHC I and Titin expression along the longitudinal myotube axis (Fig. 6B). We observed a sinusoidal variation in the density of these two proteins, perfectly colocalized as expected in a mature sarcomere, an aspect not found without stretching.

Conclusion

Stretching techniques without the use of PDMS, such as hydrogels, 3D-bioprinting, or electrospinning, have already been developed to achieve aligned myotubes with advanced fiber differentiation. These approaches are considered potential exogenous muscle grafts for muscle loss treatment. However, for mechanistic research focused on muscular response to mechanical stress, these methods do not allow for the application of a sufficiently wide range of stretch intensity. Exercise-induced mechanical stress is a double-edged sword. While it is crucial for obtaining well-differentiated fibers, it can also adversely affect myoblast differentiation, leading to the suppression of gene expressions related to muscle transcription factors such as Myog and MyoD.[66,73] In humans, there is significant inter-individual variability in the muscular response to exercise-induced damage, and substantial literature exists on polymorphisms of genes encoding key proteins in the muscle–tendon unit, which have implications for recovery from strenuous exercise, especially in elite athletes.[23,74,75] Our tool could be useful for further research in this area.

Indeed, in this study, we proposed an optimized protocol for human primary muscle-derived cells culture, enabling standardized uniaxial mechanical stress with a biocompatible organic–inorganic photostructurable hybrid material (OIPHM).

This new tool allows for easy modification of mechanical stress input and guidance of muscle fibers, facilitating the comparison, even simultaneously during the same observation, of responses to a range of mechanical constraints in human primary myoblast-derived myotubes without the need for expensive and time-consuming manufacturing technologies previously used,[27–29] such as creating a master mold, which are unsuitable for rapid prototyping.

With this approach were able to identify easily the most efficient dimensions of the PDMS microstructure regarding the height and width of the longitudinal guide grooves to generate well-differentiated and aligned human myotubes. PDMS, being a flexible and robust polymer, is perfectly suitable for modeling a variety of stretching protocols that reproduce physiological mechanical stress. Moreover, proposing a model of stretch on muscle fibers aligned in two dimensions on an easily mobilizable scaffold such as PDMS is particularly suitable for real-time observations under fluorescence microscopy, to evaluate different key aspect of stretch-induced behaviors of myogenic progenitors such as sarcomere compliance or calcium homeostasis.

The stretching protocol proposed in this study effectively stimulates human myotube growth and maturation, providing a valuable tool for future investigations into the variability among individuals in their muscle response to exercise-induced mechanical stress. This model will enable the comparison of cellular mechanisms involved in stretch-induced behaviors of myogenic progenitors from individuals with varying levels of muscular atrophy due to the same pathology.

This model will be also particularly useful in future studies evaluating muscle fiber resistance to mechanical stress-induced injuries, a hallmark of congenital myopathies with deletion in the region of titin[76] or dystrophin deficiency.[77]

Data availability

The data supporting the findings of this study are available at: **https://doi.org/10.57745/F9OKTE**. All biological data have been consolidated into a single Excel file. The raw spectrometry data from the analyses are accessible in the manufacturer's format, along with the numerical data in an Excel file. Atomic force microscopy (AFM) data have been extracted and are available in an Excel format.

Author contributions

(TR) investigation, methodology, writing original draft; (FR) software, formal analysis, validation, data curation for stretching protocol; (GS) conceptualization and resources synthesis part of the hybrid material (GC) supervision, methodology for primary cultures of human myoblasts; (GH) investigation for primary cultures of human myoblasts; (AF) investigation for micropatterned PDMS; (VH) software, validation, data curation, formal analysis for X-ray photoelectron spectroscopy and atomic force microscopy; (LR, JM, MC) investigation process for bifunctional RGD peptides; (NS) supervision for stretching protocol; (SC) supervision and investigation for the synthesis part of the hybrid material; (CE) supervision, validation, data curation, formal analysis for peptide synthesis; (PE) supervision, methodology, formal analysis, validation and software for photostructured hybrid material on silicon membranes; (SM) project administration, supervision, conceptualization, writing – original draft, writing – review & editing, funding acquisition.

Conflicts of interest

There are no conflicts to declare.

Acknowledgements

Funding came in the form of a PhD scholarship from the CNRS. This work was partly supported by the French RENATECH network and its FEMTO-ST technological facility for Alpha 110 XPS analyses. Peptide purifications were performed using the facilities of SynBio3 IBISA platform supported by IBMM and ITMO cancer. The Occitanie region funded the creation of the technological platform POMM (OptoMicrofluidic platform of Montpellier), whose equipment and expertise enabled the development of the implantation of microstructures on silicone membranes. Synvio3 equipment was publicly funded through the I-SITE Excellence Program of the University of Montpellier, under the Investissements France 2030.

References

1 S. C. Bodine and F. Edward, Adolph Distinguished Lecture, Skeletal muscle atrophy: Multiple pathways leading to a common outcome, *J. Appl. Physiol.*, 2020, **129**(2), 272–282.
2 J. R. Ruiz, X. Sui, F. Lobelo, J. R. Morrow Jr., A. W. Jackson and M. Sjöström, *et al.*, Association between muscular strength and mortality in men: prospective cohort study, *BMJ*, 2008, **337**(7661), a439.
3 E. Dent, J. E. Morley, A. J. Cruz-Jentoft, H. Arai, S. B. Kritchevsky and J. Guralnik, *et al.*, International Clinical Practice Guidelines for Sarcopenia (ICFSR): Screening, Diagnosis and Management, *J. Nutr., Health Aging*, 2018, **22**(10), 1148–1161.
4 J. H. Lautaoja, D. C. Turner, A. P. Sharples, R. Kivelä, S. Pekkala and J. J. Hulmi, *et al.*, Mimicking exercise in vitro: effects of myotube contractions and mechanical stretch on omics, *Am. J. Physiol.*, 2023, **324**(4), C886–C892.
5 A. Moustogiannis, A. Philippou, E. Zevolis, O. Taso, A. Chatzigeorgiou and M. Koutsilieris, Characterization of Optimal Strain, Frequency and Duration of Mechanical Loading on Skeletal Myotubes' Biological Responses, *In Vivo*, 2020, **34**(4), 1779–1788.
6 J. I. Andersen, C. P. Pennisi, T. Fink and V. Zachar, Focal Adhesion Kinase Activation Is Necessary for Stretch-Induced Alignment and Enhanced Differentiation of Myogenic Precursor Cells, *Tissue Eng., Part A*, 2018, **24**(7–8), 631–640.
7 A. Marom, Y. Berkovitch, S. Toume, M. B. Alvarez-Elizondo and D. Weihs, Non-damaging stretching combined with sodium pyruvate supplement accelerate migration of fibroblasts and myoblasts during gap closure, *Clin. Biomech.*, 2019, **62**, 96–103.
8 J. Brunetti, S. Koenig, A. Monnier and M. Frieden, Nanopattern surface improves cultured human myotube maturation, *Skeletal Muscle*, 2021, **11**(1), 12.
9 K.-Y. Song, J. C. Correia, J. L. Ruas and A. I. Teixeira, Effects of topological constraints on the alignment and maturation of multinucleated myotubes, *Biotechnol. Bioeng.*, 2021, **118**(6), 2234–2242.
10 Y.-C. Huang, R. G. Dennis, L. Larkin and K. Baar, Rapid formation of functional muscle in vitro using fibrin gels, *J. Appl. Physiol.*, 2005, **98**(2), 706–713.
11 S. Ast, S. Passey, L. Greensmith, V. Mudera and L. Mp, Characterization and optimization of a simple, repeatable system for the long term in vitro culture of aligned myotubes in 3D, *J. Cell. Biochem.*, 2012, **113**(3), 1044–1053.
12 W. Kim, C. H. Jang and G. H. Kim, A Myoblast-Laden Collagen Bioink with Fully Aligned Au Nanowires for Muscle-Tissue Regeneration, *Nano Lett.*, 2019, **19**(12), 8612–8620.
13 W. Kim, H. Lee, J. Lee, A. Atala, J. J. Yoo and S. J. Lee, *et al.*, Efficient myotube formation in 3D bioprinted tissue construct by biochemical and topographical cues, *Biomaterials*, 2020, **230**, 119632.
14 A. J. Khadpekar, M. Khan, A. Sose and A. Majumder, Low Cost and Lithography-free Stamp fabrication for Microcontact Printing, *Sci. Rep.*, 2019, **9**(1), 1024.
15 P. Bajaj, B. Reddy, L. Millet, C. Wei, P. Zorlutuna and G. Bao, *et al.*, Patterning the differentiation of C2C12 skeletal myoblasts, *Integr. Biol.*, 2011, **3**(9), 897–909.
16 M. M. Smoak, K. J. Hogan, K. J. Grande-Allen and A. G. Mikos, Bioinspired electrospun dECM scaffolds guide cell growth and control the formation of myotubes, *Sci. Adv.*, 2021, **7**(20), eabg4123.
17 A. E. A. Santos, T. Cotta, J. P. F. Santos, J. S. F. Camargos, A. C. C. Carmo and E. G. A. Alcântara, *et al.*, Bioactive cellulose acetate nanofiber loaded with annatto support skeletal muscle cell attachment and proliferation, *Front. Bioeng. Biotechnol.*, 2023, **11**, 1–13.
18 L. Sun, H. Chen, D. Xu, R. Liu and Y. Zhao, Developing organs-on-chips for biomedical applications, *Smart Med.*, 2024, **3**(2), e20240009.
19 Y. J. Choi, Y. J. Jun, D. Y. Kim, H. G. Yi, S. H. Chae and J. Kang, *et al.*, A 3D cell printed muscle construct with tissue-derived bioink for the treatment of volumetric muscle loss, *Biomaterials*, 2019, **206**, 160–169.
20 D. S. Veliz, K. L. Lin and C. Sahlgren, Organ-on-a-chip technologies for biomedical research and drug development: A focus on the vasculature, *Smart Med.*, 2023, **2**(1), e20220030.
21 L. Qiu, B. Kong, T. Kong and H. Wang, Recent advances in liver-on-chips: Design, fabrication, and applications, *Smart Med.*, 2023, **2**(1), e20220010.
22 V. Perez-Puyana, P. Wieringa, Y. Yuste, F. de la Portilla, A. Guererro and A. Romero, *et al.*, Fabrication of hybrid scaffolds obtained from combinations of PCL with gelatin or collagen via electrospinning for skeletal muscle tissue engineering, *J. Biomed. Mater. Res., Part A*, 2021, **109**(9), 1600–1612.
23 M. Collins and S. M. Raleigh, Genetic risk factors for musculoskeletal soft tissue injuries, *Med. Sport Sci.*, 2009, **54**, 136–149.
24 K. Faid, R. Voicu, M. Bani-Yaghoub, R. Tremblay, G. Mealing and C. Py, *et al.*, Rapid fabrication and chemical patterning of

polymer microstructures and their applications as a platform for cell cultures, *Biomed. Microdevices*, 2005, **7**(3), 179–184.

25 C. H. Hsieh, C. J. Huang and Y. Y. Huang, Patterned PDMS based cell array system: a novel method for fast cell array fabrication, *Biomed. Microdevices*, 2010, **12**(5), 897–905.

26 A. M. Almonacid Suarez, M. G. L. Brinker, L. A. Brouwer, I. van der Ham, M. C. Harmsen and P van Rijn, Topography-Mediated Myotube and Endothelial Alignment, Differentiation, and Extracellular Matrix Organization for Skeletal Muscle Engineering, *Polymers*, 2020, **12**(9), 1–21.

27 R. G. Thakar, Q. Cheng, S. Patel, J. Chu, M. Nasir and D. Liepmann, *et al.*, Cell-shape regulation of smooth muscle cell proliferation, *Biophys. J.*, 2009, **96**(8), 3423–3432.

28 C. G. Anene-Nzelu, K. Y. Peh, A. Fraiszudeen, Y. H. Kuan, S. H. Ng and Y. C. Toh, *et al.*, Scalable alignment of three-dimensional cellular constructs in a microfluidic chip, *Lab Chip*, 2013, **13**(20), 4124–4133.

29 Y. Maaref, S. Jannati, F. Jayousi, P. Lange, M. Akbari and M. Chiao, *et al.*, Developing a soft micropatterned substrate to enhance maturation of human induced pluripotent stem cell-derived cardiomyocytes, *Acta Biomater.*, 2024, **190**, 133–151.

30 Z. Chen and J. B. Lee, Biocompatibility of SU-8 and Its Biomedical Device Applications, *Micromachines*, 2021, **12**(7), 2162–2170.

31 K. V. Nemani, K. L. Moodie, J. B. Brennick, A. Su and B. Gimi, In vitro and in vivo evaluation of SU-8 biocompatibility, *Mater. Sci. Eng., C*, 2013, **33**(7), 4453–4459.

32 P. Y. Yeh, Z. Zhang, M. Lin and X. Cao, Nonfouling hydrophilic poly(ethylene glycol) engraftment strategy for PDMS/SU-8 heterogeneous microfluidic devices, *Langmuir*, 2012, **28**(46), 16227–16236.

33 J. Jabbour, S. Calas, M. Smaihi, S. Gatti and P. Etienne, Study of EETMOS hydrolysis and polycondensation by 29Si NMR spectroscopy. Application to optical 3D waveguides fabrication, *J. Non-Cryst. Solids*, 2008, **354**(10), 1001–1009.

34 R. A. Martin, S. Yue, J. V. Hanna, P. D. Lee, R. J. Newport and M. E. Smith, *et al.*, Characterizing the hierarchical structures of bioactive sol-gel silicate glass and hybrid scaffolds for bone regeneration, *Philos. Trans. R. Soc., A*, 1963, **2012**(370), 1422–1443.

35 C. Belon, X. Allonas, C. Croutxé-barghorn and J. Lalevée, Overcoming the oxygen inhibition in the photopolymerization of acrylates: A study of the beneficial effect of triphenylphosphine, *J. Polym. Sci., Part A: Polym. Chem.*, 2010, **48**(11), 2462–2469.

36 M. Oubaha, P. Etienne, S. Calas, P. Coudray, J. M. Nedelec and Y. Moreau, Sol–Gel Derived Organic and Inorganic Hybrid Materials for Photonic Applications: Contribution to the Correlation Between the Material Structure and the Transmission in the Near Infrared Region, *J. Sol-Gel Sci. Technol.*, 2005, **33**(2), 241–248.

37 J. Jabbour, S. Calas, S. Gatti, R. K. Kribich, M. Myara and G. Pille, *et al.*, Characterization by IR spectroscopy of an hybrid sol–gel material used for photonic devices fabrication, *J. Non-Cryst. Solids*, 2008, **354**(2), 651–658.

38 M. Abadie, N. Chia and F. Boey, Cure kinetics for the ultraviolet cationic polymerization of cycloliphatic and diglycidyl ether of bisphenol-A (DGEBA) epoxy systems with sulfonium salt using an auto catalytic model, *J. Appl. Polym. Sci.*, 2002, **86**, 1587–1591.

39 J. V. Crivello and U. Varlemann, Mechanistic study of the reactivity of 3,4-epoxycyclohexylmethyl 3′,4′-epoxycyclohexancarboxylate in photoinitiated cationic polymerizations, *J. Polym. Sci., Part A: Polym. Chem.*, 1995, **33**(14), 2473–2486.

40 M. Morra, E. Occhiello, R. Marola, F. Garbassi, P. Humphrey and D. Johnson, On the aging of oxygen plasma-treated polydimethylsiloxane surfaces, *J. Colloid Interface Sci.*, 1990, **137**(1), 11–24.

41 S. Bhattacharya, A. Datta, J. M. Berg and S. Gangopadhyay, Studies on surface wettability of poly(dimethyl) siloxane (PDMS) and glass under oxygen-plasma treatment and correlation with bond strength, *J. Microelectromech. Syst.*, 2005, **14**(3), 590–597.

42 K. J. M. Boonen, M. L. P. Langelaan, R. B. Polak, D. W. J. van der Schaft, F. P. T. Baaijens and M. J. Post, Effects of a combined mechanical stimulation protocol: Value for skeletal muscle tissue engineering, *J. Biomech.*, 2010, **43**(8), 1514–1521.

43 J. Martin, M. Wehbi, C. Echalier, S. Hunger, A. Bethry and X. Garric, *et al.*, Direct Synthesis of Peptide-Containing Silicones: A New Way to Bioactive Materials, *Chem. – Eur. J.*, 2020, **26**(56), 12839–12845.

44 S. Y. Boateng, S. S. Lateef, W. Mosley, T. J. Hartman, L. Hanley and B. Russell, RGD and YIGSR synthetic peptides facilitate cellular adhesion identical to that of laminin and fibronectin but alter the physiology of neonatal cardiac myocytes, *Am. J. Physiol.*, 2005, **288**(1), C30–C38.

45 I. C. Yasa, N. Gunduz, M. Kilinc, M. O. Guler and A. B. Tekinay, Basal Lamina Mimetic Nanofibrous Peptide Networks for Skeletal Myogenesis, *Sci. Rep.*, 2015, **5**, 16460.

46 E. Santos, A. Garate, J. L. Pedraz, G. Orive and R. M. Hernández, The synergistic effects of the RGD density and the microenvironment on the behavior of encapsulated cells: In vitro and in vivo direct comparative study, *J. Biomed. Mater. Res., Part A*, 2014, **102**(11), 3965–3972.

47 S. S. Lateef, S. Boateng, T. J. Hartman, C. A. Crot, B. Russell and L. Hanley, GRGDSP peptide-bound silicone membranes withstand mechanical flexing in vitro and display enhanced fibroblast adhesion, *Biomaterials*, 2002, **23**(15), 3159–3168.

48 J. Ballet, C. Biver, J.-P. Cano, F. Deliane, P. Etienne and M. Llosa, inventors; Essilor International Compagnie Generale dOptique SA, Centre National de la Recherche Scientifique CNRS, assignee, Method for preparing a photo-crosslinkable composition patent US8574818B2, 2013-11-05.

49 B. Xu, A. Magli, Y. Anugrah, S. J. Koester, R. C. R. Perlingeiro and W. Shen, Nanotopography-responsive myotube alignment and orientation as a sensitive phenotypic biomarker for Duchenne Muscular Dystrophy, *Biomaterials*, 2018, **183**, 54–66.

50 C. Echalier, C. Pinese, X. Garric, H. Van Den Berghe, E. Jumas Bilak and J. Martinez, *et al.*, Easy Synthesis of Tunable Hybrid Bioactive Hydrogels, *Chem. Mater.*, 2016, **28**(5), 1261–1265.
51 C. Pinese, S. Jebors, P. E. Stoebner, V. Humblot, P. Verdié and L. Causse, *et al.*, Bioactive peptides grafted silicone dressings: A simple and specific method, *Mater. Today Chem.*, 2017, **4**, 73–83.
52 J. H. Scofield, Hartree-Slater subshell photoionization cross-sections at 1254 and 1487 eV, *J. Electron Spectrosc. Relat. Phenom.*, 1976, **8**(2), 129–137.
53 E. Jean, D. Laoudj-Chenivesse, C. Notarnicola, K. Rouger, N. Serratrice and A. Bonnieu, *et al.*, Aldehyde dehydrogenase activity promotes survival of human muscle precursor cells, *J. Cell. Mol. Med.*, 2011, **15**(1), 119–133.
54 J. Gingras, R. M. Rioux, D. Cuvelier, N. A. Geisse, J. W. Lichtman and G. M. Whitesides, *et al.*, Controlling the Orientation and Synaptic Differentiation of Myotubes with Micropatterned Substrates, *Biophys. J.*, 2009, **97**(10), 2771–2779.
55 C. M. Nelson, R. P. Jean, J. L. Tan, W. F. Liu, N. J. Sniadecki and A. A. Spector, *et al.*, Emergent patterns of growth controlled by multicellular form and mechanics, *Proc. Natl. Acad. Sci. U. S. A.*, 2005, **102**(33), 11594–11599.
56 F. Gouzi, J. Maury, N. Molinari, P. Pomiès, J. Mercier and C. Préfaut, *et al.*, Reference values for vastus lateralis fiber size and type in healthy subjects over 40 years old: a systematic review and metaanalysis, *J. Appl. Physiol.*, 2013, **115**(3), 346–354.
57 A. Bernareggi, A. Bosutti, G. Massaria, R. Giniatullin, T. Malm and M. Sciancalepore, *et al.*, The State of the Art of Piezo1 Channels in Skeletal Muscle Regeneration, *Int. J. Mol. Sci.*, 2022, **23**(12), 1–13.
58 S. Abe, S. Rhee, O. Iwanuma, E. Hiroki, N. Yanagisawa and K. Sakiyama, *et al.*, Effect of Mechanical Stretching on Expressions of Muscle Specific Transcription Factors MyoD, Myf-5, Myogenin and MRF4 in Proliferated Myoblasts, *Anat., Histol., Embryol.*, 2009, **38**(4), 305–310.
59 Y.-J. Chang, Y.-J. Chen, C.-W. Huang, S.-C. Fan, B.-M. Huang and W.-T. Chang, *et al.*, Cyclic Stretch Facilitates Myogenesis in C2C12 Myoblasts and Rescues Thiazolidinedione-Inhibited Myotube Formation, *Front. Bioeng. Biotechnol.*, 2016, **4**, 2162–2170.
60 C. P. Pennisi, C. G. Olesen, M. de Zee, J. Rasmussen and V. Zachar, Uniaxial cyclic strain drives assembly and differentiation of skeletal myocytes, *Tissue Eng., Part A*, 2011, **17**(19–20), 2543–2550.
61 O. Iwanuma, S. Abe, E. Hiroki, S. Kado, K. Sakiyama and A. Usami, *et al.*, Effects of Mechanical Stretching on Caspase and IGF-1 Expression During the Proliferation Process of Myoblasts, *Zool. Sci.*, 2008, **25**(3), 242–247.
62 D. G. Moon, G. Christ, J. D. Stitzel, A. Atala and J. J. Yoo, Cyclic Mechanical Preconditioning Improves Engineered Muscle Contraction, *Tissue Eng., Part A*, 2008, **14**(4), 473–482.
63 K. W. Aguilar-Agon, A. J. Capel, N. R. W. Martin, D. J. Player and M. P. Lewis, Mechanical loading stimulates hypertrophy in tissue-engineered skeletal muscle: Molecular and phenotypic responses, *J. Cell. Physiol.*, 2019, **234**(12), 23547–23558.
64 Q. A. Soltow, E. H. Zeanah, V. A. Lira and D. S. Criswell, Cessation of cyclic stretch induces atrophy of C2C12 myotubes, *Biochem. Biophys. Res. Commun.*, 2013, **434**(2), 316–321.
65 A. Ilaiwy, M. T. Quintana, J. R. Bain, M. J. Muehlbauer, D. I. Brown and W. E. Stansfield, *et al.*, Cessation of biomechanical stretch model of C2C12 cells models myocyte atrophy and anaplerotic changes in metabolism using non-targeted metabolomics analysis, *Int. J. Biochem. Cell Biol.*, 2016, **79**, 80–92.
66 S. H. Kook, Y. O. Son, K. C. Choi, H. J. Lee, W. T. Chung and I. H. Hwang, Cyclic mechanical stress suppresses myogenic differentiation of adult bovine satellite cells through activation of extracellular signal-regulated kinase, *Mol. Cell. Biochem.*, 2008, **309**(1–2), 133–141.
67 S. M. Somers, N. Y. Zhang, J. B. F. Morrissette-McAlmon, K. Tran, H.-Q. Mao and W. L. Grayson, Myoblast maturity on aligned microfiber bundles at the onset of strain application impacts myogenic outcomes, *Acta Biomater.*, 2019, **94**, 232–242.
68 X. Qiu, Z. Deng, M. Wang, Y. Feng, L. Bi and L. Li, Piezo protein determines stem cell fate by transmitting mechanical signals, *Hum. Cell*, 2023, **36**(2), 540–553.
69 H. P. Ortuste Quiroga, M. Ganassi, S. Yokoyama, K. Nakamura, T. Yamashita and D. Raimbach, *et al.*, Fine-Tuning of Piezo1 Expression and Activity Ensures Efficient Myoblast Fusion during Skeletal Myogenesis, *Cell*, 2022, **11**(3), 1–21.
70 T. Shirakawa, T. Toyono, A. Inoue, T. Matsubara, T. Kawamoto and S. Kokabu, Factors Regulating or Regulated by Myogenic Regulatory Factors in Skeletal Muscle Stem Cells, *Cell*, 2022, **11**(9), 1–14.
71 P. G. De Deyne, Formation of sarcomeres in developing myotubes: role of mechanical stretch and contractile activation, *Am. J. Physiol.*, 2000, **279**(6), C1801–C1811.
72 X. Chen, W. Du, Z. Cai, S. Ji, M. Dwivedi and J. Chen, *et al.*, Uniaxial Stretching of Cell-Laden Microfibers for Promoting C2C12 Myoblasts Alignment and Myofibers Formation, *ACS Appl. Mater. Interfaces*, 2020, **12**(2), 2162–2170.
73 J. S. Otis, T. J. Burkholder and G. K. Pavlath, Stretch-induced myoblast proliferation is dependent on the COX2 pathway, *Exp. Cell Res.*, 2005, **310**(2), 417–425.
74 N. Yang, D. G. MacArthur, J. P. Gulbin, A. G. Hahn, A. H. Beggs and S. Easteal, *et al.*, ACTN3 genotype is associated with human elite athletic performance, *Am. J. Hum. Genet.*, 2003, **73**(3), 627–631.
75 M. J. Laguette, Y. Abrahams, S. Prince and M. Collins, Sequence variants within the 3′-UTR of the COL5A1 gene alters mRNA stability: implications for musculoskeletal soft tissue injuries, *Matrix Biol.*, 2011, **30**(5–6), 338–345.
76 K. Nishikawa, S. L. Lindstedt, A. Hessel and D. Mishra, N2A Titin: Signaling Hub and Mechanical Switch in Skeletal Muscle, *Int. J. Mol. Sci.*, 2020, **21**(11), 1–18.
77 B. J. Petrof, J. B. Shrager, H. H. Stedman, A. M. Kelly and H. L. Sweeney, Dystrophin protects the sarcolemma from stresses developed during muscle contraction, *Proc. Natl. Acad. Sci. U. S. A.*, 1993, **90**(8), 3710–3714.

